

Visible-light induced one-pot hydrogenation and amidation of nitroaromatics with carboxylic acids over 2D MXene-derived Pt/N-TiO₂/Ti₃C₂

Heyan Jiang^{*}, Zujie Hu, Chuan Gan, Bin Sun, Shuzhen Kong, Fengxia Bian^{*}

Key Laboratory of Catalysis Science and Technology of Chongqing Education Commission, Chongqing Key Laboratory of Catalysis and New Environmental Materials, College of Environmental and Resources, Chongqing Technology and Business University, Chongqing, 400067, China

ARTICLE INFO

Keywords:

Photocatalysis
One-pot tandem reaction
Platinum
Amidation
MXene

ABSTRACT

Pt nanoparticles supported on N doped titanium dioxide/titanium carbide (MXene) heterojunctions were employed as photocatalysts for the tandem reactions between aromatic nitro compounds and carboxylic acids to produce amide products. The 3%Pt/N-TiO₂/Ti₃C₂ heterojunction was prepared by in situ grew TiO₂ on Ti₃C₂ nanosheets and then N doped TiO₂ with melamine, Pt nanoparticles with 3.3 nm mean diameter well dispersed on N-TiO₂/Ti₃C₂. 3%Pt/N-TiO₂/Ti₃C₂ had excellent amidation activity and chemoselectivity under visible-light irradiation. The elevated catalytic performance of 3%Pt/N-TiO₂/Ti₃C₂ was owing to the improvement in photogenerated electron and hole separation efficiency through charge short-range directional transmission caused by the intimate contact between the TiO₂ and the conductive Ti₃C₂. This direct hydrogenation along with amidation between nitroaromatics and carboxylic acids own actual merits in the amides produce with no harmful byproducts. In situ DRIFTS spectra verified that the amidation activation with visible light irradiation at 25 °C was much faster than heating.

Introduction

Amides are a standout amongst functional groups in naturally-occurring molecules or modern organic synthesis, and they are being widely used by pharmaceutical chemists [1–4]. Conventional methods of amide synthesis include the dicyclohexylcarbodiimide (DCC)/N, N'-carbonyldiimidazoles activation, or the reaction of amines with acid halides, acid anhydrides, esters, acyl azides, etc. [5–7]. Toxic reagents, sensitivity, poor atomic economy as well as complex purification processes are significant disadvantages of these methods. It is well known that the most preferred method of amide synthesis is direct condensation amine with carboxylic acid, and amine used herein is usually produced through nitro compound catalytic hydrogenation. However, because of the non-reactive ammonium carboxylate intermediate, the direct condensation process required rather high temperature [8–11]. So, amide synthesis avoiding poor atom economy was considered as the top challenge in organic chemistry [12–16]. At present, several methods for directly synthesizing amides from carboxylic acids and amines without using coupling agent have been reported. Such as, N-heterocyclic carbene catalyzed amidation by means of the formation of activated

carboxylates. This amidization by using small amount of catalysts provided a solution to the problem of the formation of recognized by-products in conventional amide synthesis [17,18]. The boron-based catalysts were considered to be one of the most outstanding in the synthesis of amides with a waste-free catalytic manner [19–21]. Nonetheless, it is still not easy to separate the product from the homogeneous catalytic reaction mixture. It is worth highlighting that Gu et al. [22] used Pt nanowires for the one pot reaction between aromatic nitro compounds and carboxylic acid to synthesize amide directly under mild conditions with excellent recyclability and no toxic byproducts.

The pursuit of high efficiency along with minimal waste-generating new environment-friendly reaction processes has become one of the most important targets in chemistry [23,24]. One-pot tandem/cascade reactions, generally require multifunctional catalysts with diverse catalytically active sites in a site-isolated way to keep their independent function, allow multiple steps to occur in single pot without the need to separate the intermediates, providing great advantages and arousing extensive research interest [25–27]. Utilizing light to drive synthetic process is rather attractive among one-pot tandem/cascade reactions [28–31]. MXenes is a rising 2D transition metal carbide and/or

^{*} Corresponding authors.

E-mail addresses: orgjiang@163.com (H. Jiang), bianqian1201@163.com (F. Bian).

<https://doi.org/10.1016/j.mcat.2021.111490>

Received 20 November 2020; Received in revised form 1 February 2021; Accepted 14 February 2021

Available online 2 March 2021

2468-8231/© 2021 Elsevier B.V. All rights reserved.

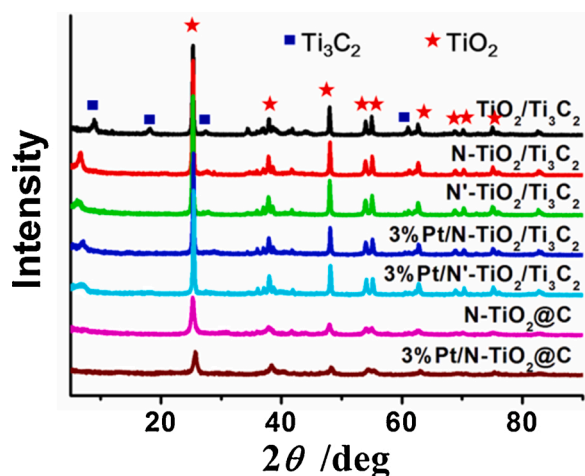


Fig. 1. XRD patterns of $\text{TiO}_2/\text{Ti}_3\text{C}_2$, $\text{N-TiO}_2/\text{Ti}_3\text{C}_2$, $\text{N}'\text{-TiO}_2/\text{Ti}_3\text{C}_2$, $3\%\text{Pt}/\text{N-TiO}_2/\text{Ti}_3\text{C}_2$, $3\%\text{Pt}/\text{N}'\text{-TiO}_2/\text{Ti}_3\text{C}_2$, $\text{N-TiO}_2@\text{C}$ and $3\%\text{Pt}/\text{N-TiO}_2@\text{C}$.

carbonitride with a general formula $\text{M}_{n+1}\text{X}_n\text{T}_x$ ($n = 1, 2, 3$; $\text{T}_x = \text{OH}, \text{O}, \text{F}$ group) [32,33]. Owing to the excellent structure and chemical properties, MXenes have been extensively studied during the past few years [34–39]. MXene has excellent electron conductivity which makes it easier to transfer charge from the semiconductor to MXene and improves the separation efficiency of electron and hole thus achieving directional charge transmission [40,41]. With above unique nature, MXene is viewed as one of the most promising photocatalytic material.

Herein, we report Pt nanoparticles supported on N doped titanium dioxide/titanium carbide (MXene) ($3\%\text{Pt}/\text{N-TiO}_2/\text{Ti}_3\text{C}_2$) heterojunctions as photocatalysts for the tandem reactions between aromatic nitro compounds and carboxylic acids to produce amide products. The $3\%\text{Pt}/\text{N-TiO}_2/\text{Ti}_3\text{C}_2$ heterojunctions was formed by in situ grew TiO_2 on Ti_3C_2 nanosheets and then N doped TiO_2 with melamine; Pt nanoparticles with small diameter were well separated on $\text{N-TiO}_2/\text{Ti}_3\text{C}_2$ subsequently. $3\%\text{Pt}/\text{N-TiO}_2/\text{Ti}_3\text{C}_2$ exhibited excellent amidation activity and chemoselectivity under visible-light irradiation. In comparison, Pt nanoparticles on N doped titanium dioxide prepared from titanium carbide ($3\%\text{Pt}/\text{N-TiO}_2@\text{C}$) had apparently decreased activity and chemoselectivity to amides. The improved catalytic property of $3\%\text{Pt}/\text{N-TiO}_2/\text{Ti}_3\text{C}_2$ should be ascribed to the improvement in photogenerated

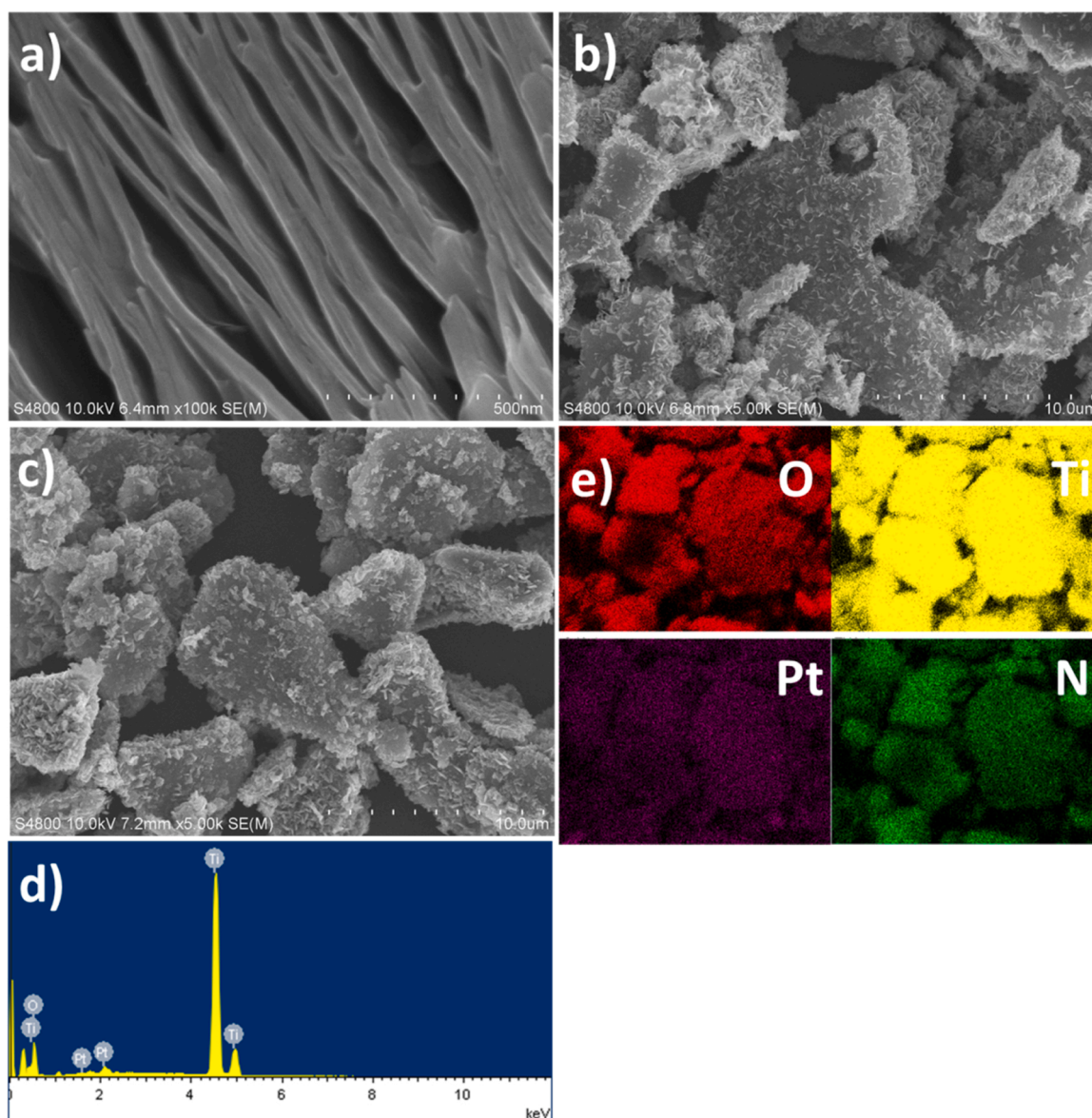


Fig. 2. SEM images of a) Ti_3C_2 ; b) $\text{N-TiO}_2/\text{Ti}_3\text{C}_2$; c) $3\%\text{Pt}/\text{N-TiO}_2/\text{Ti}_3\text{C}_2$. EDS spectrum d) and mapping images e) of $3\%\text{Pt}/\text{N-TiO}_2/\text{Ti}_3\text{C}_2$.

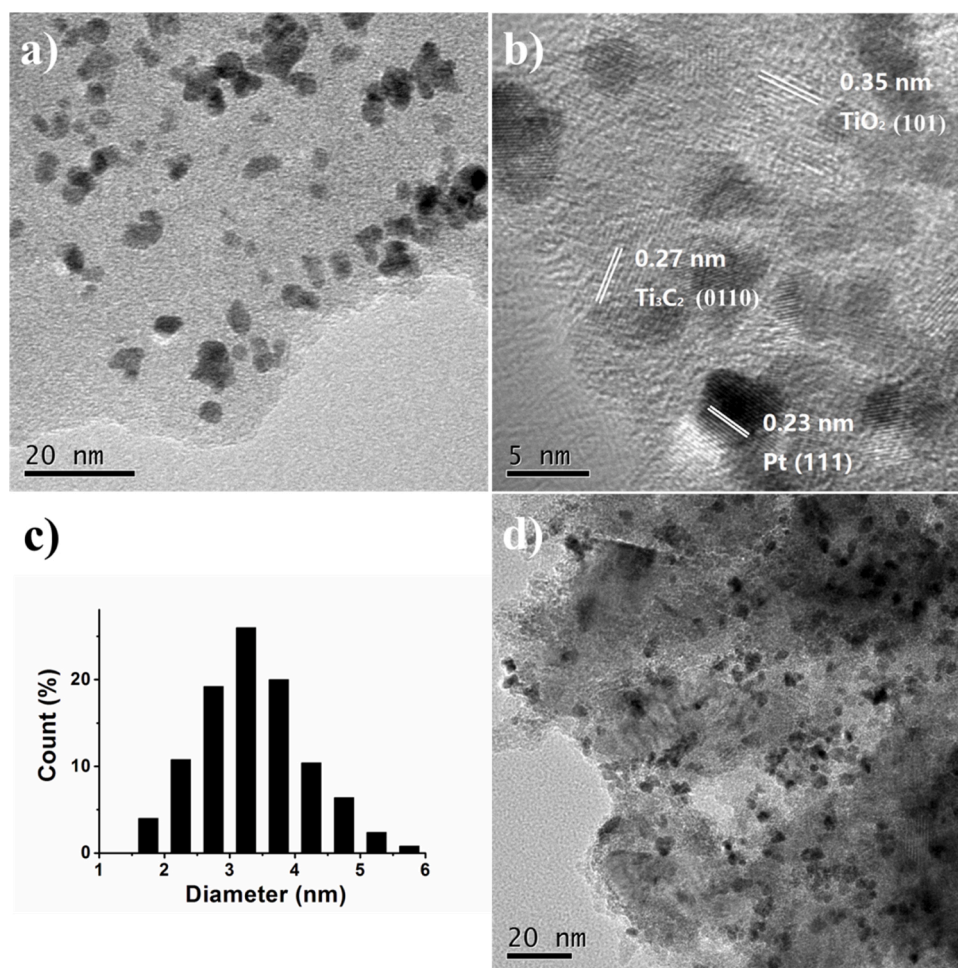


Fig. 3. TEM image a), HRTEM image b) and TEM image after three consecutive recycles d) of 3%Pt/N-TiO₂/Ti₃C₂.

electron and hole separation efficiency through charge short-range directional transmission caused by the intimate contact between the TiO₂ and the conductive Ti₃C₂. The waste-free catalytic manner to direct hydrogenation along with amidation between nitroaromatics and carboxylic acids own actual merits in the amides production, furthermore, sheds light on the possibility for development multifunctional catalysis in a broad range of visible-light prompted organic synthesis.

Results and discussion

The XRD patterns of all prepared catalytic materials were employed to characterize the crystal phase and phase purity in Fig. 1. Consistent with the literature [42,43], the layered TiO₂/Ti₃C₂ heterojunction was successfully prepared on the layered Ti₃C₂ nanosheets by hydrothermal oxidation. The coexistence of the peak of anatase TiO₂ and the peak of Ti₃C₂ indicated successfully partial oxidation of Ti₃C₂ nanosheets [42, 43]. After TiO₂/Ti₃C₂ was N doped with melamine or urea (N-TiO₂/Ti₃C₂ or N'-TiO₂/Ti₃C₂), the peak intensity of Ti₃C₂ in N-TiO₂/Ti₃C₂ or N'-TiO₂/Ti₃C₂ was further declined in comparison with TiO₂/Ti₃C₂, and the (002) diffraction peak of Ti₃C₂ shifted to lower angle, indicating that two-dimensional material structural expansion happened during the N doping [36]. The melamine or urea doping did not change the lattice morphology of anatase TiO₂. There had no other impurity phase except the diffraction peak of TiO₂. This indicated that N dopant atoms were directly incorporated into the crystal lattice of TiO₂ and did not form related compounds or other precipitation phase [44–46]. Meanwhile, no diffraction peak of melamine was observed, indicating that melamine or urea had been completely decomposed. Further loading of the metal Pt,

no significant Ti₃C₂ peak shift was detected, indicating that the loading of the Pt NPs did not change the structure of N-TiO₂/Ti₃C₂ or N'-TiO₂/Ti₃C₂. The XRD spectrum of 3%Pt/N-TiO₂/Ti₃C₂ or 3% Pt/N'-TiO₂/Ti₃C₂ had no obvious diffraction peak of Pt, indicating the small Pt NPs were well dispersed on N-TiO₂/Ti₃C₂ or N'-TiO₂/Ti₃C₂. For comparison, no characteristic peak of Ti₃C₂ was detected in N-TiO₂@C. Similar to the case in the 3%Pt/N-TiO₂/Ti₃C₂ catalyst, the melamine doping did not change the lattice morphology of anatase TiO₂ in N-TiO₂@C and small Pt NPs were well dispersed on N-TiO₂@C.

In the FTIR spectrum (Fig. S2 in supporting information), all Ti₃C₂Tx derived TiO₂/Ti₃C₂, N-TiO₂/Ti₃C₂, 3%Pt/N-TiO₂/Ti₃C₂, N-TiO₂@C and 3%Pt/N-TiO₂@C showed a broad band in 400–800 cm⁻¹, which should be owing to the characteristic of Ti-O-Ti. With the N doping of TiO₂/Ti₃C₂, the Ti-O-Ti vibration was enhanced due to the Ti₃C₂ further oxidation [47]. Another absorption at around 1635 cm⁻¹ was the hydroxyl group bending vibrations, and the intensity of the hydroxyl group bending vibrations peak became reinforced from TiO₂/Ti₃C₂ to N-TiO₂/Ti₃C₂. This indicated the N doping could construct more hydroxyl groups on the surface of the catalytic material. After Pt NPs loading, the hydroxyl group bending vibrations red shift was observed, which indicated the coordination between the hydroxyl group and Pt NPs.

Fig. 2a was scanning electron microscope (SEM) image of stacked layer Ti₃C₂ [36]. Fig. 2b was SEM image of melamine doped TiO₂/Ti₃C₂ (N-TiO₂/Ti₃C₂) with characteristic of uniformly grown melamine doped TiO₂ on the surface and the interlayer of the Ti₃C₂ MXene layer. The surface of the N-TiO₂/Ti₃C₂ became rougher and the stacked layers became thicker in comparison with Ti₃C₂, indicating that 2D Ti₃C₂ was

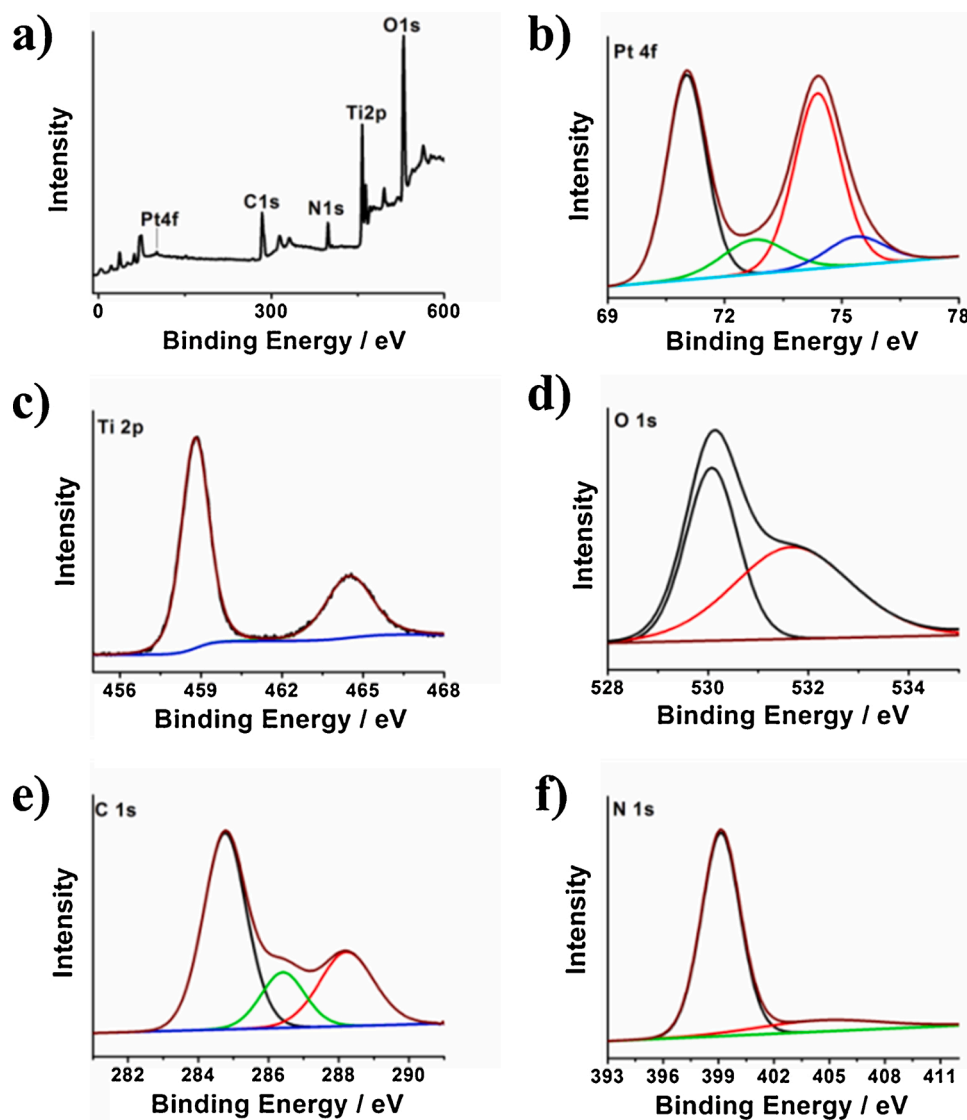


Fig. 4. XPS spectra of 3%Pt/N-TiO₂/Ti₃C₂: a) full scan, b) Pt 4f, c) Ti 2p, d) O 1s e) C 1s and f) N 1s.

effectively encapsulated by N-TiO₂. After Pt loading and reduction to nanoparticles (Fig. 2c and Fig. S1a), 3%Pt/N-TiO₂/Ti₃C₂ almost maintained the feature as observed in N-TiO₂/Ti₃C₂ because of the Ti₃C₂ support. On the other hand, without Ti₃C₂ support, no evident stacked layers were observed in 3%Pt/N-TiO₂@C (Fig. S1b). Energy dispersive X-ray spectroscopy spectra (EDS) and corresponding mapping of 3%Pt/N-TiO₂/Ti₃C₂ were illustrated in Fig. 2d and e. O, Ti, Pt and N could be evidently observed, and these elements coexisted uniformly in the sample proving the successful doping of N to TiO₂.

Transmission electron microscopy (TEM) was employed to characterize detailed information about metal Pt NPs on N-TiO₂/Ti₃C₂. The TEM image of 3%Pt/D-TiO₂/Ti₃C₂ (Fig. 3a) clearly appeared that Pt nanoparticles with the average diameter of 3.3 nm were uniformly distributed on N-TiO₂/Ti₃C₂. Although after in-situ growth of TiO₂, doping and Pt metal NPs support process, N-TiO₂ and Pt metal NPs covered most of the Ti₃C₂ surface, but the lattice fringes of Pt NPs (0.23 nm), N-TiO₂ (0.27 nm) along with Ti₃C₂ (0.35 nm) [36] were simultaneously observed in high-resolution transmission electron micrographs (Fig. 3b), which guaranteed that Pt NPs, N-TiO₂ nanocrystals as well as Ti₃C₂ could be adequately contacted with the reactants and played the role of active centers in the photocatalytic reaction.

The XPS analysis was employed to elucidate the nature of 3%Pt/N-TiO₂/Ti₃C₂. XPS characterization showed the presence of platinum,

titanium, oxygen, carbon and nitrogen (Fig. 4a), which signified the successful preparation of heterojunction. Pt 4f were deconvoluted into two species, binding energies 70.9 and 74.3 eV were the 4f_{7/2} and 4f_{5/2} peaks of metallic Pt; 72.6 and 75.8 eV were the 4f_{7/2} and 4f_{5/2} peaks of Pt(II) (Fig. 4b) [48,49]. This suggested that metallic Pt was the main species along with the existence of a small amount of Pt(II) [49,50]. The spectrum of Ti 2p region of 3%Pt/N-TiO₂/Ti₃C₂ catalyst was presented in Fig. 4c. In comparison with TiO₂, Ti2p (458.8 and 464.3 eV) in the 3%Pt/N-TiO₂/Ti₃C₂ shifted negatively. The peak shifted to lower binding energy might be owing to the doping resulted in the formation of O-Ti-N band in the lattice [51]. XPS spectrum of O 1s (Fig. 4d) could be deconvoluted into two oxygen components at 530.1 eV (Ti—O—Ti) and 531.7 eV (Ti—OH) [44]. C 1s in Fig. 4e could be fitted to three peaks at 284.7 eV (C—C bond); 286.4 eV, which was assigned to C—O bond [52]; and 288.2 eV, which was assigned to Ti—O—C because of substitution of carbon atoms into titanium lattice and was also detected in some other Ti₃AlC₂ derivative materials [53,54]. XPS spectra of N 1s in Fig. 4f had two peaks at 399.2 and 404.5 eV. 399.2 eV should be ascribed to the existence of lattice oxygen replaced by N atom (O—Ti—N) [51].

To clarify the intrinsic reason for the excellent performance of 3%Pt/N-TiO₂/Ti₃C₂, light-harvesting capability was carried out. The light absorption ability of N-TiO₂/Ti₃C₂, N-TiO₂@C, 3%Pt/N-TiO₂/Ti₃C₂ along with 3%Pt/N-TiO₂@C samples were characterized by UV-vis

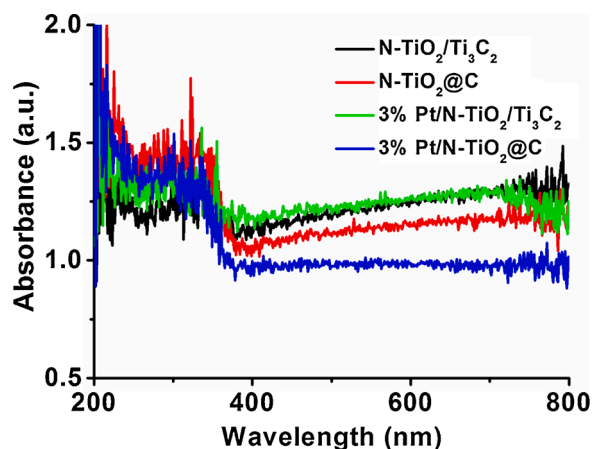


Fig. 5. UV-vis absorption spectra of N-TiO₂/Ti₃C₂, N-TiO₂@C, 3%Pt/N-TiO₂/Ti₃C₂ and 3%Pt/N-TiO₂@C.

absorption spectroscopy (Fig. 5). Generally, the light absorption by N-TiO₂@C and 3%Pt/N-TiO₂@C was lower than that of N-TiO₂/Ti₃C₂ and 3%Pt/N-TiO₂/Ti₃C₂. The absorption of 3%Pt/N-TiO₂/Ti₃C₂ after Pt NPs loading was increased compared to material N-TiO₂/Ti₃C₂, however, in contrast with N-TiO₂@C, the 3%Pt/N-TiO₂@C light absorption was declined.

Photocurrent generation and electrochemical impedance spectroscopy were carried out to evaluate the charge separation and transfer efficiency between N-TiO₂/Ti₃C₂, 3%Pt/N-TiO₂/Ti₃C₂ and 3%Pt/N-TiO₂@C [55]. Fig. 6a was a transient photocurrent graph of photocatalysts on ITO electrode with visible light illumination. The photocurrent response of the N-TiO₂/Ti₃C₂, 3%Pt/N-TiO₂/Ti₃C₂ as well as 3%Pt/N-TiO₂@C electrodes was rapid, stable and repeatable during lighting on/off cycles. The photocurrent of 3%Pt/N-TiO₂/Ti₃C₂ was higher than that of N-TiO₂/Ti₃C₂, which indicated that the introduction of strong electron accepting Pt NPs to N-TiO₂/Ti₃C₂ could enhance the separation of photo-generated electrons and holes. On the other hand, 3%Pt/N-TiO₂/Ti₃C₂ with visible light exhibited superior photocurrent than 3%Pt/N-TiO₂@C, suggesting the undoubted synergy between N-TiO₂ and Ti₃C₂. Ti₃C₂ acting as the transporter for electrons significantly improved the separation ability of photo-generated charge carriers [43]. The smaller radius of the arc in the electrochemical impedance spectrum represented smaller electron transfer resistance on the surface of photoelectrode, which as a rule brought about more efficient separation of photoelectron-hole pairs as well as speedier interfacial charge transfer. In Fig. 7b, the circular segment span of the EIS Nyquist curve was 3%Pt/N-TiO₂/Ti₃C₂ < 3%Pt/N-TiO₂@C < N-TiO₂/Ti₃C₂, which represented that the resistance of the interface charge transfer from the electrode to the electrolyte molecule. The results of the electrochemical impedance spectroscopy echo the law of photocurrent test.

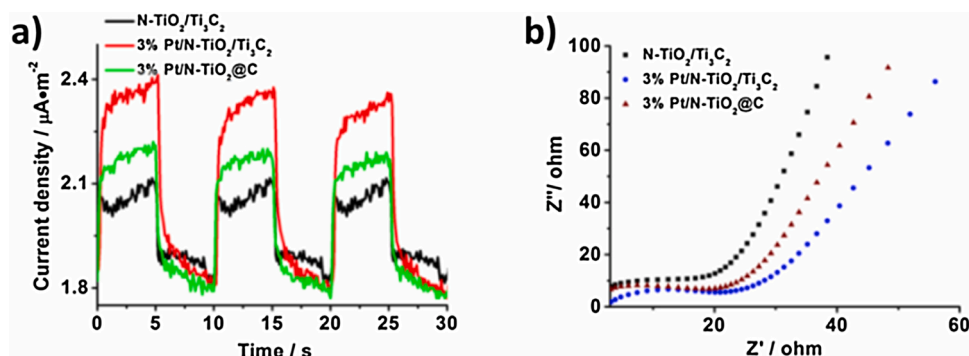


Fig. 6. Transient photocurrent responses a) and electrochemical impedance spectroscopy b) of N-TiO₂/Ti₃C₂, 3%Pt/N-TiO₂/Ti₃C₂ and 3%Pt/N-TiO₂@C.

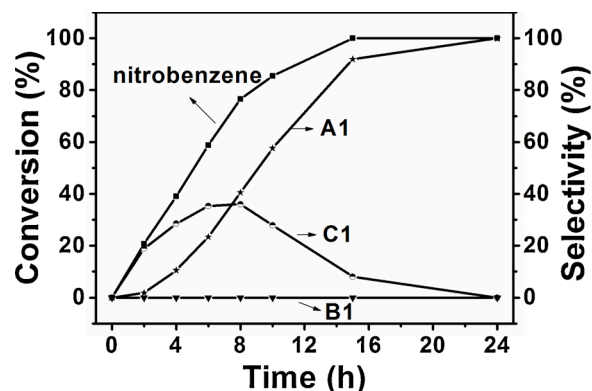


Fig. 7. Time-dependent catalytic performance in visible light promoted one-pot hydrogenation and amidation of nitrobenzene with acetic acid over 3%Pt/N-TiO₂/Ti₃C₂. The reaction conditions are the same as in Table 1 entry 3.

Table 1

Visible light promoted one-pot hydrogenation and amidation of nitrobenzene with acetic acid over Pt NPs on N doped TiO₂/MXene Ti₃C₂ heterojunctions.^a

Entry	Catalyst	main product		
		Conv. / %	A1 sel. / %	C1 sel. / %
1	–	–	–	–
2 ^b	3%Pt/N-TiO ₂ /Ti ₃ C ₂	100.0	64.0	36.0
3	3%Pt/N-TiO ₂ /Ti ₃ C ₂	100.0	100.0	–
4 ^c	3%Pt/N-TiO ₂ /Ti ₃ C ₂	99.0	95.0	5.0
5 ^d	3%Pt/N-TiO ₂ /Ti ₃ C ₂	100.0	100.0	–
6 ^e	3%Pt/N-TiO ₂ /Ti ₃ C ₂	31.0	29.0	71.0
7 ^f	3%Pt/N-TiO ₂ /Ti ₃ C ₂	–	–	–
8 ^g	3%Pt/N-TiO ₂ /Ti ₃ C ₂	54.0	81.9	18.1
9 ^h	3%Pt/N-TiO ₂ @C	67.6	86.7	13.3

^a Reaction conditions: nitrobenzene (1 mmol) K₃PO₄ (1 mmol) and solvent (3 mL) were stirred magnetically under 1 atm H₂ in a reaction tube in the presence of Pt NPs on N doped TiO₂/Ti₃C₂ heterojunction catalysts with substrate: Pt = 600 for 24 h, melamine:TiO₂/Ti₃C₂ = 0.5:1 during the doping, 0.75 W cm⁻² blue LED, no B1 was detected in Table 1, “–” = no product or negligible product. ^b no K₃PO₄. ^c melamine:TiO₂/Ti₃C₂ = 0.25:1 during the doping. ^d melamine:TiO₂/Ti₃C₂ = 1:1 during the doping. ^e 0.15 W cm⁻² blue LED instead. ^f without visible light irradiation. ^g urea instead of melamine during the doping. ^h N-TiO₂@C instead of N-TiO₂/Ti₃C₂.

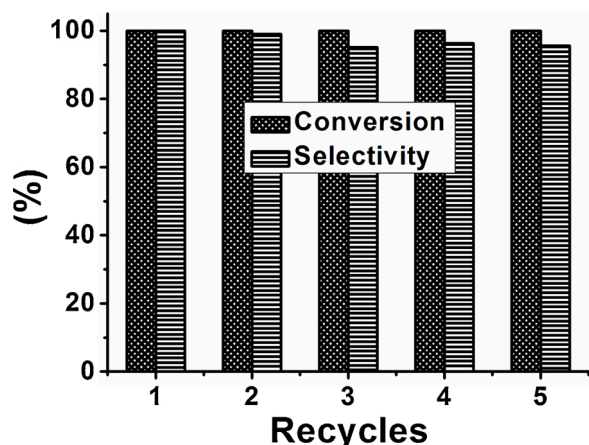


Fig. 8. Cycling visible light promoted one-pot hydrogenation and amidation of nitrobenzene with acetic acid over 3%Pt/N-TiO₂/Ti₃C₂. The reaction conditions are the same as in Table 1 entry 3.

The as-prepared 3%Pt/N-TiO₂/Ti₃C₂ catalyst was used for one-pot hydrogenation and amidation of nitro compounds with carboxylic acids under visible light irradiation. Nitrobenzene and acetic acid was chosen to test the catalytic performance (Table 1). No product was detected without catalyst (Table 1, entry 1). Without alkaline additive K₃PO₄, one-pot hydrogenation and amidation of nitrobenzene was absolutely converted but just with 64.0 % chemoselectivity to acetanilide (A1) (Table 1, entry 2), which suggested that the base was required for the deprotonation of amine [56]. The decreased conversion in the absence of base should be owing to aniline (a primary amine) itself could assist the progress of reaction by acting as a base. In the presence of K₃PO₄ additive, hydrogenation and amidation reaction could reach 100 % conversion with 100 % chemoselectivity to A1 (Table 1, entry 3). The amount of melamine used during TiO₂/Ti₃C₂ doping was further optimized (Table 1, entries 3–5). When the melamine:TiO₂/Ti₃C₂ increased from 0.25:1 to 0.5:1 during the doping, slightly increase in activity and chemoselectivity was observed. Further increase the melamine:TiO₂/Ti₃C₂ ratio had no obvious influence on the catalytic performance. Above results indicated that N doping (N 2p generate new energy levels by hybridizing with O 2p, thus reducing the apparent band gap) with appropriate amount of melamine could effectively form hybrid energy levels in the TiO₂ band gap [57]. To gain deep insight into the role of light on the reaction, we investigated the hydrogenation and amidation reaction with 0.15 W cm⁻² blue LED, just 31.0 % conversion with 29.0 % chemoselectivity to A1 was achieved (Table 1, entry 6). The one-pot hydrogenation and amidation reaction could not be carried out

without visible light irradiation (Table 1, entry 7). For comparison, urea doped TiO₂/Ti₃C₂ was also tested as the carrier, poor activity and moderate chemoselectivity to acetanilide was attained (Table 1, entry 8). In comparison with 3%Pt/N-TiO₂/Ti₃C₂, 3%Pt/N-TiO₂@C reached 67.6 % conversion and 86.7 % chemoselectivity to A1. This result indicated that the combination of Ti₃C₂, TiO₂ and Pt NPs together with the formation of heterojunction, with Ti₃C₂ acting as a transporter for electrons to inhibit the backward diffusion of electrons, significantly improved one-pot nitrobenzene hydrogenation as well as amidation with acetic acid. We further monitored the reaction between nitrobenzene and acetic acid with 1 atm hydrogen over visible light promoted photocatalysis (Fig. 7). Nitrobenzene was firstly reduced to aniline intermediate followed closely with amidation. No other byproduct was detected. The 3%Pt/N-TiO₂/Ti₃C₂ could be reused by straightforward centrifugation followed by vacuum drying. Catalyst could be recycled 5 times with no obvious activity and chemoselectivity decrease (Fig. 8). No obvious Pt loss was detected by ICP-OES in the reaction solution.

In the visible light induced 3%Pt/N-TiO₂/Ti₃C₂ catalytic system, nitrobenzene one-pot hydrogenation and amidation with carboxylic acids could also be extended to various carboxylic acids (Table 2). 3% Pt/N-TiO₂/Ti₃C₂ showed excellent activity and chemoselectivity to corresponding amides (>90 %) with acetic acid, propanoic acid, butyric acid, valeric acid as well as isobutyric acid (Table 2, entries 1, 3–6). However, formic acid, with lower pKa value of 3.77, gave lower chemoselectivity to the corresponding amide (Table 2, entry 2); meanwhile, octanoic acid gave a chemoselectivity of 27.9 % and aniline was the byproduct (Table 2, entry 7). Either the chemoselectivity decrease for formic acid or the photocatalytic decline for octanoic acid should be ascribed to the steric hindrance.

To further extend the scope of the use of aromatic nitro compounds in the one-pot hydrogenation and amidation with atmosphere H₂ upon visible light irradiated 3%Pt/N-TiO₂/Ti₃C₂, other aromatic nitro compounds having different substituents were chosen as substrates (Table 3), good to excellent activity and chemoselectivity were achieved. When the aromatic nitro compounds all had methyl substituent (Table 3, entries 2–4), the chemoselectivity order, *o*-nitrotoluene < *m*-nitrotoluene < *p*-nitrotoluene, should be ascribed to the steric hindrance effect. As for stronger electron-donating methoxy substituent substrates, *o*-nitroanisole showed 99.8 % chemoselectivity to corresponding amide (Table 3, entry 5). However, only 85.3 % chemoselectivity was obtained with *p*-nitroanisole (Table 3, entry 6), this should be explained that both electron donating as well as steric hindrance effect were favorable for the *p*-nitroanisole conversion, and the monoamidation product was further converted into bisamidation product (Table 3, entry 6). For the electron withdrawing group substituted nitrobenzenes, the slightly chemoselectivity decrease to corresponding amides should be owing to the electronic effect (Table 3, entries 7–9). Additionally, *m*-

Table 2

Visible light promoted one-pot hydrogenation and amidation of nitrobenzene with carboxylic acids over 3%Pt/N-TiO₂/Ti₃C₂.^a

Entry	Substrate	Conv. / %	A sel. / %	B sel. / %	C sel. / %
1	acetic acid	100.0	100.0	–	–
2	formic acid	100.0	85.8	14.2	–
3	propionic acid	99.8	91.9	–	8.1
4	butyric acid	100.0	96.1	–	3.9
5	valeric acid	95.2	93.6	–	6.4
6	isobutyric acid	100.0	90.8	–	9.2
7	octanoic acid	95.4	27.9	–	72.1

^a The reaction conditions were the same as in Table 1 (entry 3) except the carboxylic acids.

Table 3Visible light promoted one-pot hydrogenation and amidation of nitroaromatics with acetic acid over 3%Pt/N-TiO₂/Ti₃C₂.^a

Entry	Substrate	Conv. / %	A sel. / %	B sel. / %	C sel. / %
1		100.0	100.0	–	–
2		96.4	95.8	–	0.6
3		100.0	99.7	–	0.3
4		100.0	100.0	–	–
5		100.0	99.8	–	0.2
6		100.0	85.3	14.7	–
7		99.0	91.5	–	8.5
8		100.0	94.3	–	5.7
9		100.0	90.6	–	9.4
10		100.0	89.5	–	10.5
11		100.0	98.5	–	1.5

^a The reaction conditions were the same as in Table 1 (entry 3) except the nitroaromatics.

nitroacetophenone and *p*-nitrobenzaldehyde could be converted to corresponding amides with 89.5 % and 98.5 % chemoselectivity respectively (Table 3, entries 10–11).

Some experiments were carried out to explore the photocatalytic one-pot hydrogenation and amidation reaction mechanism (Table 4). Rather low photocatalytic activity and chemoselectivity to A1 were achieved with 3%Pt/Ti₃C₂ (Table 4, entry 2), which indicated that the introduction of doped TiO₂ in the catalytic system was necessary for the efficient light utilization. In comparison with 3%Pt/N-TiO₂/Ti₃C₂, 3% Pt/N-TiO₂@C exhibited lower activity and chemoselectivity to A1 (Table 4, entry 3 vs 1), which should be explained that Ti₃C₂ acted as a transporter for electrons to accelerate the nitrobenzene one-pot hydrogenation and amidation with acetic acid. When e⁻ scavenger KBrO₃ was introduced to the catalytic system, photocatalytic activity was obviously decreased (Table 4, entry 4), and nitrobenzene reduction should be accelerated by photogenerated electrons. On the other hand, when h⁺ scavenger TEOA was introduced to the catalytic system,

chemoselectivity to A1 was decreased (Table 4, entry 5), therefore, amidation step should be promoted by photogenerated holes in some degree. When acetic acid and H₂O were used as the reaction solvent, amidation step was obviously inhibited (Table 4, entry 6), which evidenced that photocatalytic amidation step went through a dehydration process. Considering the reaction temperature might have decisive influence on the chemoselectivity in the hydrogenation and amidation catalytic reaction [22], we further tested the thermal catalytic performance of 3%Pt/D-TiO₂/Ti₃C₂ at 60 °C or 80 °C (Table 4, entries 7–8). Rather low activity with complete chemoselectivity to aniline was obtained at 60 °C; and just 12.6 % conversion and 47.6 % chemoselectivity to amidation product was attained at 80 °C. Considering the actual photocatalytic system temperature was lower than 60 °C with the LED irradiation, the excellent photocatalytic one-pot hydrogenation and amidation performance should reasonably be attributed to the improved catalytic system activation efficiency with visible light.

To gain insight view about how the catalytic system achieved highly

Table 4

Experimental probes on one-pot hydrogenation and amidation reaction mechanism.^a

Entry	Condition changes	Conv. / %	A1 sel. / %	C1 sel. / %
1	No	100.0	100.0	–
2	3%Pt/Ti ₃ C ₂ as catalyst	4.7	57.0	43.0
3	3%Pt/D-TiO ₂ @C as catalyst	60.6	81.0	19.0
4	100 μM KBrO ₃ as e ⁻ scavenger	27.0	89.5	10.5
5	100 μM TEOA as h ⁺ scavenger	90.0	80.8	19.2
6	Solvent: acetic acid:H ₂ O = 1:1	100.0	6.3	93.7
7	Dark, 60 °C	5.7	–	100.0
8	Dark, 80 °C	12.6	47.6	52.4

^a The reaction conditions were the same as in Table 1 entry 3.

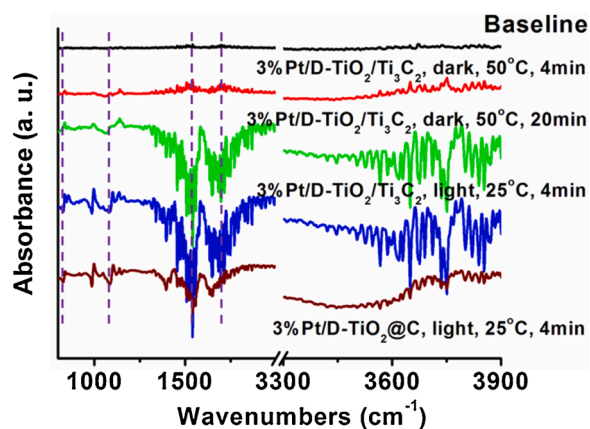
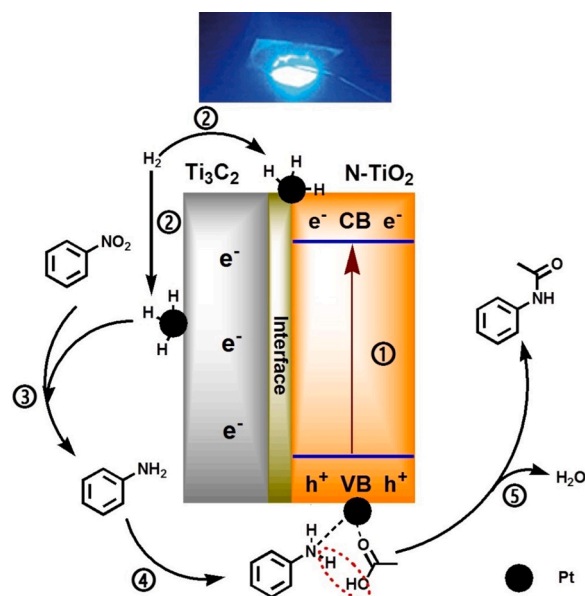


Fig. 9. In situ DRIFTS spectra for one-pot hydrogenation and amidation of aniline with acetic acid over 3%Pt/N-TiO₂/Ti₃C₂ and 3%Pt/N-TiO₂@C under visible light irradiation or heating.

efficient activation under the visible light irradiation, we used the in situ diffuse reflectance infrared fourier transform spectroscopy (DRIFTS) to dynamically observe along with analyze the primary difference in amidation activation of the catalytic system over 3%Pt/N-TiO₂/Ti₃C₂ and 3%Pt/N-TiO₂@C under visible light irradiation or heating (Fig. 9). The baseline spectrum was tested before light irradiation or heating. The following characteristic peaks decrease was primary observed in the in situ DRIFTS with light irradiation or heating. The absorption peak around 850 cm⁻¹ was the out-of-plane deformation vibration of N–H bond in substrate aniline; the absorption at about 1100 cm⁻¹ was the hydroxyl group deformation vibration in carboxylic acid; the absorption at about 1570 cm⁻¹ was the in-plane deformation vibration of N–H; 1700 cm⁻¹ was the telescopic vibration of C=O in carboxylic acid and the absorption peak between 3500 cm⁻¹ and 3900 cm⁻¹ was N–H telescopic vibration [58,59]. In the presence of 3%Pt/N-TiO₂/Ti₃C₂ catalyst at 50 °C, hydroxyl group deformation vibration, N–H in-plane deformation vibration, C=O telescopic vibration as well as N–H telescopic vibration, which were related to the amidation catalytic activation, gradually weakened with the increase of heating time. On the other side, the decrease in deformation vibration of hydroxyl group, in-plane deformation vibration of N–H bond, telescopic vibration of C=O as well as telescopic vibration of N–H under visible light irradiation at 25 °C was much faster than heating. In addition, the decrease in out-of-plane deformation vibration of N–H bond in substrate aniline was also observed under visible light irradiation. The comparison of



Scheme 1. Proposed mechanism for visible light promoted one-pot hydrogenation and amidation of nitrobenzene with acetic acid over 3%Pt/N-TiO₂/Ti₃C₂.

visible light illumination and heating in catalytic system indicated that the visible light irradiation promoted catalytic activation efficiency of both aniline and carboxylic acid, which should be the basic reason for the evident selective amidation catalytic efficiency improvement under visible light irradiation. 3%Pt/N-TiO₂@C catalyst was also tested under similar conditions. Without the Ti₃C₂ electron transporter, the decrease in in-plane deformation vibration of N–H bond, telescopic vibration of C=O in carboxylic acid as well as telescopic vibration of N–H became not that obvious, indicating the decrease in the amino and carboxyl group activation and leading to lower amidation catalytic efficiency.

Based on above discussion, visible light promoted hydrogenation and amidation of nitrobenzene with acetic acid over 3%Pt/N-TiO₂/Ti₃C₂ was given (Scheme 1). Electrons and holes could be generated with visible light irradiation of N-TiO₂/Ti₃C₂. Short-range charge directional transmission construction with electron transporter Ti₃C₂ and metal NPs supported on N-TiO₂/Ti₃C₂ could lead to efficient electron transfer from excited N-TiO₂/Ti₃C₂ to metal NPs [43,60]. Electron-rich Pt specie was formed by the transfer of photogenerated electrons to Pt nanoparticles with visible-light irradiation of 3%Pt/N-TiO₂/Ti₃C₂ (①); Hydrogen from H–H bond cleavage (②) was transferred to electron-rich Pt to form Pt hydride, and then the selective hydrogenation of nitro was conducted (③). Considering the N–H, C=O as well as O–H activation observed with in situ DRIFTS spectra, the amidation activation model was proposed on Pt NPs (④): Absorbed aniline could be activated by photoinduced holes on the valence band [61]; and holes left on the 3%Pt/N-TiO₂/Ti₃C₂ support could also assist the cleavage of the C–OH bond in carboxyl group [62]. With the synergy action of visible light, Pt NPs as well as holes generated with visible light irradiation, the intermediate removed water to realize the amidation conversion (⑤).

Conclusion

Pt nanoparticles supported on N doped titanium dioxide/titanium carbide (MXene) (3%Pt/N-TiO₂/Ti₃C₂) heterojunctions, formed by in situ grew TiO₂ on Ti₃C₂ nanosheets, N doped TiO₂ with melamine, and then Pt nanoparticles with small diameter well dispersed on N-TiO₂/Ti₃C₂, were employed as photocatalysts for the tandem reactions between aromatic nitro compounds and carboxylic acids to produce amide products. In comparison with the excellent amidation activity and chemoselectivity over 3%Pt/N-TiO₂/Ti₃C₂, Pt nanoparticles on N doped titanium dioxide prepared from titanium carbide (3%Pt/N-TiO₂@C) had

apparently decreased activity and chemoselectivity to amides. The improved catalytic performance over 3%Pt/N-TiO₂/Ti₃C₂ was ascribed to the improvement in photogenerated electron and hole separation efficiency through charge short-range directional transmission caused by the intimate contact between the TiO₂ and the conductive Ti₃C₂. The waste-free catalytic manner to direct hydrogenation along with amidation between nitroaromatics and carboxylic acids was achieved via a successful coupling of the 2D transition metal carbide/carbonitride based photocatalysis, Ti₃C₂ based short-range directional charge transmission as well as Pt NPs based hydrogenation along with amidation under rather mild conditions. In situ DRIFTS spectra further verified that the amidation activation with visible light irradiation at 25 °C was much faster than heating. This work also shed light on the infinite possibilities for development multifunctional catalysis for a broad range of visible-light promoted organic transformations.

CRedit authorship contribution statement

Heyan Jiang: Conceptualization, Investigation, Data curation, Writing - review & editing, Funding acquisition. **Zujie Hu:** Investigation, Data curation. **Chuan Gan:** Investigation, Validation. **Bin Sun:** Conceptualization, Methodology. **Shuzhen Kong:** Supervision, Funding acquisition. **Fengxia Bian:** Supervision, Funding acquisition.

Declaration of Competing Interest

The authors declare that they have no known competing financial interests or personal relationships that could have appeared to influence the work reported in this paper.

Acknowledgements

This work was financially supported by Natural Science Foundation Project of CQ (No. cstc2018jcyjAX0735, cstc2019jcyj-msxmX0641, cstc2015jcyjBX0031), National Natural Science Foundation of China (No.212011184), Ministry of Education of Chongqing (No. KJQN201900811), Chongqing Technology and Business University (950119090) and Chongqing Key Laboratory of Catalysis and New Environmental Materials (KFJJ2019082), Key Disciplines of Chemical Engineering and Technology in Chongqing Colleges and Universities during the 13th Five Year Plan and Innovation Group of New Technologies for Industrial Pollution Control of Chongqing Education Commission (CXQT19023).

Appendix A. Supplementary data

Supplementary material related to this article can be found, in the online version, at doi:<https://doi.org/10.1016/j.mcat.2021.111490>.

References

- [1] V.R. Pattabiraman, J.W. Bode, *Nature* 480 (2011) 471–479.
- [2] M.T. Sabatini, L.T. Boulton, H.F. Sneddon, T.D. Sheppard, *Nat. Catal.* 2 (2019) 10–17.
- [3] R.M. de Figueiredo, J.S. Suppo, J.M. Campagne, *Chem. Rev.* 116 (2016) 12029–12122.
- [4] R.N. Lima, C.S. dos Anjos, E.V.M. Orozco, A.L.M. Porto, *Mol. Catal.* 466 (2019) 75–105.
- [5] E. Bouron, G. Goussard, C. Marchand, M. Bonin, X. Pannecoucke, J.C. Quirion, H. P. Husson, *Tetrahedron Lett.* 40 (1999) 7227–7230.
- [6] U. Ragnarsson, L. Grehn, *Acc. Chem. Res.* 31 (1998) 494–501.
- [7] F. Fazio, C.H. Wong, *Tetrahedron Lett.* 44 (2003) 9083–9085.
- [8] L.J. Goossen, D.M. Ohlmann, P.P. Lange, *Synthesis* (2008) 160–164.
- [9] L. Perreux, A. Loupy, F. Volatron, *Tetrahedron* 58 (2002) 2155–2162.
- [10] H. Charville, D. Jackson, G. Hodges, A. Whiting, *Chem. Commun.* 46 (2010) 1813–1823.
- [11] F. De Schouwer, L. Claes, A. Vandekerckhove, J. Verduyck, D.E. De Vos, *ChemSusChem* 12 (2019) 1272–1303.
- [12] V.V. Gaikwad, P.A. Mane, S. Dey, D. Patel, B.M. Bhanage, *Mol. Catal.* 482 (2020), 110672.
- [13] X. Wang, *Nat. Catal.* 2 (2019) 98–102.
- [14] H. Lundberg, F. Tinnis, N. Selander, H. Adolfsson, *Chem. Soc. Rev.* 43 (2014) 2714–2742.
- [15] Z. Dong, Z. Ren, S.J. Thompson, Y. Xu, G. Dong, *Chem. Rev.* 117 (2017) 9333–9403.
- [16] Y.C. Chu, S.W. Bi, X.H. Wu, Y.Y. Jiang, Y.X. Liu, B.P. Ling, X.A. Yuan, *Mol. Catal.* 497 (2020), 111222.
- [17] K.D. Schleicher, T.F. Jamison, *Org. Lett.* 9 (2007) 875–878.
- [18] C. Zhang, J. Liu, C. Xia, *Catal. Sci. Technol.* 5 (2015) 4750–4754.
- [19] K. Ishihara, S. Ohara, H. Yamamoto, *J. Org. Chem.* 61 (1996) 4196–4197.
- [20] T.B. Nguyen, J. Sorres, M.Q. Tran, L. Ermolenko, A. Al-Mourabit, *Org. Lett.* 14 (2012) 3202–3205.
- [21] H. Charville, D. Jackson, G. Hodges, A. Whiting, *Chem. Commun.* 46 (2010) 1813–1823.
- [22] M. Li, L. Hu, X.Q. Cao, H.Y. Hong, J.M. Lu, H.W. Gu, *Chem. Eur. J.* 17 (2011) 2763–2768.
- [23] C.J. Clarke, W.C. Tu, O. Levers, A. Brohl, J.P. Hallett, *Chem. Rev.* 118 (2018) 747–800.
- [24] N. Lucas, L. Gurrula, S.B. Halligudi, *Mol. Catal.* 490 (2020), 110966.
- [25] H. Ghafari, G. Jafari, A. Rashidzadeh, F. Manteghi, *Mol. Catal.* 475 (2019), 110491.
- [26] A.H. Chowdhury, I.H. Chowdhury, S. Biswas, S.M. Islam, *Mol. Catal.* 493 (2020), 111050.
- [27] S. Zhang, J. Xu, H. Cheng, C. Zang, B. Sun, H. Jiang, F. Bian, *Appl. Catal. A Gen.* 596 (2020), 117536.
- [28] H. Jiang, J. Xu, S. Zhang, H. Cheng, C. Zang, F. Bian, *Catal. Sci. Technol.* 10 (2020), <https://doi.org/10.1039/D0CY01881C>.
- [29] H. Cheng, X. Long, F. Bian, C. Yang, X. Liu, H. Jiang, *J. Catal.* 389 (2020) 121–131.
- [30] J. Xu, S. Zhang, X. Liu, F. Bian, H. Jiang, *Catal. Sci. Technol.* 9 (2019) 6938–6945.
- [31] S. Song, J.F. Qu, P.J. Han, M.J. Hulsey, G.P. Zhang, Y.Z. Wang, S. Wang, D.Y. Chen, J.M. Lu, N. Yan, *Nat. Commun.* 11 (2020) 4899.
- [32] M. Naguib, O. Mashtalir, J. Carle, V. Presser, J. Lu, L. Hultman, Y. Gogotsi, M. W. Barsoum, *ACS Nano* 6 (2012) 1322–1331.
- [33] M. Naguib, V.N. Mochalin, M.W. Barsoum, Y. Gogotsi, *Adv. Mater.* 26 (2014) 992–1005.
- [34] M. Nasrollahzadeh, Z. Nezafat, M.G. Gorab, M. Sajjadi, *Mol. Catal.* 484 (2020), 110758.
- [35] B. Anasori, M.R. Lukatskaya, Y. Gogotsi, *Nat. Rev. Mater.* 2 (2017) 16098.
- [36] M. Ming, Y. Ren, M. Hu, Y. Zhang, T. Sun, Y. Ma, X. Li, W. Jiang, D. Gao, J. Bi, G. Fan, *Appl. Catal. B* 210 (2017) 462–469.
- [37] G.Y. Fan, X.J. Li, Y.L. Ma, Y. Zhang, J.T. Wu, B. Xu, T. Sun, D.J. Gao, J. Bi, *New J. Chem.* 41 (2017) 2793–2799.
- [38] T.P. Nguyen, D.M.T. Nguyen, D.L. Tran, H.K. Le, D.V.N. Vo, S.S. Lam, R.S. Varma, M. Shokouhimehr, C.C. Nguyen, Q.V. Le, *Mol. Catal.* 486 (2020), 110850.
- [39] H. Jiang, C. Zang, Y. Zhang, W. Wang, C. Yang, B. Sun, Y. Shen, F. Bian, *Catal. Sci. Technol.* 10 (2020) 5964–5972.
- [40] X. Chia, M. Pumera, *Nat. Catal.* 1 (2018) 909–921.
- [41] T. Su, R. Peng, Z.D. Hood, M. Naguib, I.N. Ivanov, J.K. Keum, Z. Qin, Z. Guo, Z. Wu, *ChemSusChem* 11 (2018) 688–699.
- [42] C. Peng, X.F. Yang, Y.H. Li, H. Yu, H.J. Wang, F. Peng, *ACS Appl. Mater. Inter.* 8 (2016) 6051–6060.
- [43] Y. Xu, S. Wang, J. Yang, B. Han, R. Nie, J. Wang, J. Wang, H. Jing, *Nano Energy* 51 (2018) 442–450.
- [44] Q. Liu, L. Ai, J. Jiang, *J. Mater. Chem. A* 6 (2018) 4102–4110.
- [45] R. Asahi, T. Morikawa, T. Ohwaki, K. Aoki, Y. Taga, *Science* 293 (2001) 269–271.
- [46] Z. Zhang, Z. Huang, X. Cheng, Q. Wang, Y. Chen, P. Dong, X. Zhang, *Appl. Surf. Sci.* 355 (2015) 45–51.
- [47] J.I. Chen, E. Loso, N. Ebrahim, G.A. Ozin, *J. Am. Chem. Soc.* 130 (2008) 5420–5421.
- [48] Q. Sun, J. Wang, X. Wang, J. Dai, X.S. Wang, H.C. Fan, Z.W. Wang, H. Li, X. Huang, W. Huang, *Nanoscale* 12 (2020) 16987–16994.
- [49] B.Y. Xia, B. Wang, H.B. Wu, Z. Liu, X. Wang, X.W. Lou, *J. Mater. Chem.* 22 (2012) 16499–16505.
- [50] Y. Wei, J. Jiao, Z. Zhao, W. Zhong, J. Li, J. Liu, G. Jiang, A. Duan, *J. Mater. Chem. A* 3 (2015) 11074–11085.
- [51] D. Ma, Y. Xin, M. Gao, J. Wu, *Appl. Catal. B* 147 (2014) 49–57.
- [52] Z. Huang, Z. Gao, S. Gao, Q. Wang, Z. Wang, B. Huang, Y. Dai, *Chinese J. Catal.* 38 (2017) 821–830.
- [53] P. Dhanasekaran, S.V. Selvaganes, S.D. Bhat, *J. Power Sources* 304 (2016) 360–372.
- [54] W. Yuan, L. Cheng, Y. Zhang, H. Wu, S. Lv, L. Chai, X. Guo, L. Zheng, *Adv. Mater. Interfaces* (2017), 1700577.
- [55] S. Zhang, J. Xu, H. Cheng, C. Zang, F. Bian, B. Sun, Y. Shen, H. Jiang, *ChemSusChem* 13 (2020) 5264–5272.
- [56] S. Karthik, R. Sreedharan, T. Gandhi, *ChemistrySelect* 4 (2019) 175–180.
- [57] R. Asahi, T. Morikawa, T. Ohwaki, K. Aoki, Y. Taga, *Science* 293 (2001) 269–271.
- [58] V. Gupta, N. Chaudhary, R. Srivastava, G.D. Sharma, R. Bhardwaj, S. Chand, *J. Am. Chem. Soc.* 133 (2011) 9960–9963.
- [59] Z. Li, W.T. Tysoe, *Sur. Sci.* 606 (2012) 1934–1941.
- [60] D.R. Sun, W.J. Liu, Y.H. Fu, Z.X. Fang, F.X. Sun, X.Z. Fu, Y.F. Zhang, Z.H. Li, *Chem. Eur. J.* 20 (2014) 4780–4788.
- [61] W. Phasayavan, M. Japa, S. Pornsuwan, D. Tantraviwat, F. Kiear, V.B. Golovko, S. Jungstuiwong, B. Inceesungvorn, *J. Colloid Interf. Sci.* 581 (2021) 719–728.
- [62] Z.F. Jiao, Y.M. Tian, B. Zhang, C.H. Hao, Y. Qiao, Y.X. Wang, Y. Qin, U. Radius, H. Braunschweig, T.B. Marder, X.N. Guo, X.Y. Guo, *J. Catal.* 389 (2020) 517–524.